An *XRCC4* Splice Mutation Associated With Severe Short Stature, Gonadal Failure, and Early-Onset Metabolic Syndrome

Christiaan de Bruin,* Verónica Mericq,* Shayne F. Andrew, Hermine A. van Duyvenvoorde, Nicole S. Verkaik, Monique Losekoot, Aleksey Porollo, Hernán Garcia, Yi Kuang, Dan Hanson, Peter Clayton, Dik C. van Gent, Jan M. Wit, Vivian Hwa, and Andrew Dauber†

Context: Severe short stature can be caused by defects in numerous biological processes including defects in IGF-1 signaling, centromere function, cell cycle control, and DNA damage repair. Many syndromic causes of short stature are associated with medical comorbidities including hypogonadism and microcephaly.

Objective: To identify an underlying genetic etiology in two siblings with severe short stature and gonadal failure.

Design: Clinical phenotyping, genetic analysis, complemented by in vitro functional studies of the candidate gene.

Setting: An academic pediatric endocrinology clinic.

Patients or Other Participants: Two adult siblings (male patient [P1] and female patient 2 [P2]) presented with a history of severe postnatal growth failure (adult heights: P1, −6.8 SD score; P2, −4 SD score), microcephaly, primary gonadal failure, and early-onset metabolic syndrome in late adolescence. In addition, P2 developed a malignant gastrointestinal stromal tumor at age 28.

Intervention(s): Single nucleotide polymorphism microarray and exome sequencing.

Results: Combined microarray analysis and whole exome sequencing of the two affected siblings and one unaffected sister identified a homozygous variant in *XRCC4* as the probable candidate variant. Sanger sequencing and mRNA studies revealed a splice variant resulting in an in-frame deletion of 23 amino acids. Primary fibroblasts (P1) showed a DNA damage repair defect.

Conclusions: In this study we have identified a novel pathogenic variant in *XRCC4*, a gene that plays a critical role in non-homologous end-joining DNA repair. This finding expands the spectrum of DNA damage repair syndromes to include XRCC4 deficiency causing severe postnatal growth failure, microcephaly, gonadal failure, metabolic syndrome, and possibly tumor predisposition. **(*J Clin Endocrinol Metab* 100: E789–E798, 2015)**

Normal growth is a hallmark of childhood health, and perturbations in a multitude of biological processes can lead to pathological growth patterns. Numerous conditions exist that present with prominent pre- and postnatal growth retardation. These conditions may be due to primary skeletal abnormalities, in which case they typically present with disproportionate short stature and skeletal dysplasia. Alternatively, there are many nonskel-

ISSN Print 0021-972X ISSN Online 1945-7197
Printed in U.S.A.

Received January 12, 2015. Accepted March 2, 2015.
First Published Online March 5, 2015

* C.d.B. and V.M. contributed equally.
† Author affiliations are shown at the bottom of the next page.
Abbreviations: BMI, body mass index; CNV, Copy Number Variation; DSB, double-stranded DNA break; GIST, gastrointestinal stromal tumor; MMEJ, microhomology-mediated end-joining; MOPD, microcephalic osteodysplastic primordial dwarfism; MPD, microcephalic primordial dwarfism; NHEJ, nonhomologous end-joining; NK, natural killer; OFC, occipital frontal circumference; OGTT, oral glucose tolerance test; P1, patient 1; P2, patient 2; PBMC, peripheral blood mononuclear cell; ROH, runs of homozygosity; S1, (unaffected) sister; SDS, SD score; SNP, single nucleotide polymorphism.

etal conditions that lead to significant proportionate short stature. At the extreme end of the spectrum lies microcephalic primordial dwarfism (MPD), a heterogeneous group of monogenic growth disorders consisting of severe intrauterine and postnatal growth restriction, leading to extreme short stature and disproportionate microcephaly (1). Prominent examples of MPD include Seckel syndrome, microcephalic osteodysplastic primordial dwarfism (MOPD) types 1 and 2, and Meier-Gorlin syndrome. In addition to classic MPD, milder syndromic growth disorders include 3M syndrome, Russell-Silver syndrome, Cockayne syndrome, Bloom syndrome, and others. Many of these disorders do not have microcephaly as a prominent component and may not have as severe prenatal growth restriction, although the phenotypes are highly variable. Each syndrome may include specific dysmorphic features and the occurrence of comorbid conditions such as primary gonadal failure, insulin resistance, or developmental delay. Within the last decade, multiple genetic etiologies have been identified for these disorders, including defects in many fundamental biological processes such as IGF-1 signaling, cell cycle regulation, DNA replication, centrosome function, maintenance of microtubule and genome integrity, and DNA damage repair (1–13) among others.

In this study we present two siblings with a novel syndrome consisting of severe short stature, microcephaly, hypergonadotropic hypogonadism, and early-onset metabolic syndrome, as well as possible tumor susceptibility caused by an underlying *XRCC4* mutation, a gene involved in the nonhomologous end-joining (NHEJ) DNA damage repair process.

Case Descriptions

Patient 1

Patient 1 (P1) is a male born at term small for gestational age, with a birth length of 45.0 cm (−2.8 SD score [SDS]) but a normal birth weight of 2.92 kg (−1.3 SDS). He showed progressive growth failure throughout childhood (Figure 1A). His body mass index (BMI) was always within normal limits for age. He had bilateral cryptorchidism, with right orchiopexy at age 7 years and atrophy of the left testicle with a volume less than 1 cc. Hemithyroidectomy for multinodular goiter was performed at age 10. He subsequently had a mildly elevated TSH with normal T_4 and was started on low-dose levothyroxine supplementation.

He presented at age 13 with absent pubertal signs, micropenis with a stretched penile length of 3.5 cm, and a baseline T level of 10 ng/dL (Table 1). He failed to enter puberty spontaneously but did not return for pubertal evaluation until the age of 18. At that time, laboratory analysis was consistent with primary gonadal failure with marked hypergonadotropic hypogonadism. Bone age was delayed by 4 years, and he was started on im T replacement therapy. He was variably compliant with T therapy and thus had poor virilization and did not reach final adult height until his mid-20s.

At the age of 16, he underwent an oral glucose tolerance test (OGTT) with a normal fasting blood glucose of 81 mg/dL and 2-hour blood glucose of 120 mg/dL. However, his insulin levels were significantly elevated (fasting, 33.7 μIU/mL; 2-h, 219 μIU/mL). At age 27, he was diagnosed with diabetes with negative anti-islet cell antibodies. He began metformin and insulin therapy in subsequent years, but due to poor compliance his hemoglobin A1c levels were consistently elevated. He was diagnosed with dyslipidemia, which was treated with a statin. At age 37, he underwent cataract surgery.

His most recent physical examination at age 39.9 years shows severe short stature (127.4 cm, −6.8 SDS), microcephaly with an occipital frontal circumference (OFC) of 51.3 cm (−3.3 SDS), a BMI of 20.3 kg/m^2 (−1.0 SDS), acanthosis, clinodactyly, small testes (<2 mL), and a high-pitched voice (Figure 1C). He has always had low-normal hemoglobin levels and never showed clinical signs of immune deficiency. He had mild lymphopenia, and lymphocyte subpopulation analysis revealed a reduced number of natural killer (NK) and B cells with a mild decrease in CD4+ T cells, however, with normal numbers of CD8+ T cells. Complement analysis showed that C3 was mildly elevated, with a normal C4 level. His IgG, IgA, and IgM levels were all normal, but the IgE was elevated (Table 1).

Patient 2

Patient 2 (P2), a sister of P1, was born with a short birth length of 46 cm (−2.3 SDS) and a birth weight of 2600 g (−1.9 SD). She was first brought to medical attention at the age of 2 years for progressive growth failure, similar to her older brother (Figure 1B). She failed to enter puberty

Cincinnati Center for Growth Disorders (C.d.B., S.F.A., V.H., A.D.), Division of Endocrinology, Cincinnati Children's Hospital Medical Center, Cincinnati, Ohio 45229; Institute of Maternal and Child Research (V.M.), Faculty of Medicine, University of Chile, 226-3 Santiago, Chile; Laboratory for Diagnostic Genome Analysis (H.A.v.D., M.L.), Department of Clinical Genetics, Leiden University Medical Center, 2333 ZA Leiden, The Netherlands; Department of Genetics (N.S.V., D.C.v.G.), Erasmus MC, 3015 CE Rotterdam, The Netherlands; Center for Autoimmune Genomics and Etiology (A.P.), Cincinnati Children's Hospital Medical Center, Cincinnati, Ohio 45229; Pediatrics Division (H.G.), Faculty of Medicine, Pontificia Universidad Catolica de Chile Santiago, 340 Santiago, Chile; Division of Developmental Biology (Y.K.), Cincinnati Children's Hospital Medical Center, Cincinnati, Ohio 45229; Institute of Human Development (D.H., P.C.), University of Manchester and Manchester Academic Health Sciences Centre, Manchester M13 9PL, United Kingdom; and Department of Pediatrics (J.M.W.), Leiden University Medical Center, 2333 ZA Leiden, The Netherlands

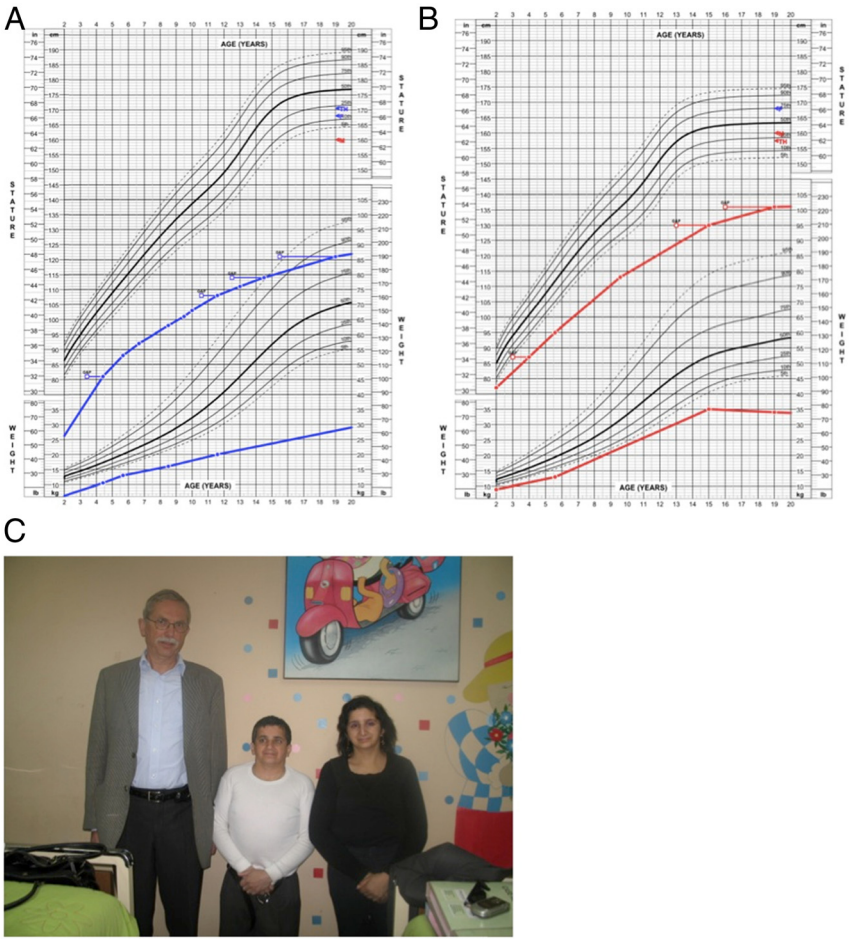

Figure 1. A and B, Height and weight curves from ages 2–20 in P1 (A, blue lines) and P2 (B, red lines). The corrected skeletal age, as determined by serial bone age assessments (Greulich and Pyle,) is depicted by the open squares. C, Photograph of P1 (middle), P2 (right), and one of the study authors (left, 176 cm) in 2009, in which both patients show severe short stature, microcephaly, and short necks.

spontaneously and was diagnosed with severe gonadal failure (hypergonadotropic hypogonadism) at age 16 (Table 1). She was started on estrogen replacement therapy, but due to poor compliance, she displayed persistent hypogonadism at age 19 with Tanner 1 breast development, Tanner 2 pubic hair, and absent axillary hair.

An OGTT performed at age 16 showed normal glucose tolerance with a fasting glucose of 81 mg/dL and a 2-hour glucose of 137 mg/dL. Similar to her brother, she demonstrated marked insulin resistance (fasting insulin, 28 μIU/mL; 2-h insulin level, 180 μIU/mL). At age 19, she was noted to have acanthosis on examination. As an adult, she had multiple elevated fasting blood sugars (peak, 154 mg/dL), but she never received medical therapy for diabetes. She also had significant dyslipidemia, which was untreated.

Unlike her brother, she did not have a history of cataract and/or thyroid surgery. She had a persistent anemia of unknown origin throughout childhood and young adulthood but no other signs of hematological or immunological disease. There was no history of frequent infections. She had normal Ig levels, with a mild elevation in C3 but normal C4. She did not have lymphocyte subsets performed.

At age 30, she was evaluated for left abdominal pain, which demonstrated a jejunal wall tumor 5 cm in diameter that was surgically removed. Pathological analysis was consistent with a gastrointestinal stromal tumor (GIST), and no adjuvant treatment was given at the time because of its benign prognosis. She did not have a history of acute radiation exposure or an increased cumulative radiation dose through repeated medical imaging before this diagnosis. At age 31, she returned to the oncology clinic and was found to have diffuse intra-abdominal metastases. Multiple thyroid nodules were also reported on ultrasound, but no tissue was obtained for analysis. She was started on imatinib therapy but was subsequently switched to sunitinib due to worsening of anemia and gastrointestinal side effects. Despite the tyrosine-kinase inhibitor treatment, the tumor continued to progress, resulting in her demise at age 36. Before her demise, her adult physical examination was remarkable for severe short stature (height, 137.4 cm; −4.0 SDS), microcephaly (head circumference, 50.5 cm; −2.9 SDS), micrognathia, triangular facies, high-pitched voice, short neck, clinodactyly, and acanthosis nigricans (Figure 1C).

Family history

The family is from rural Chile. The parents conceived a total of six children. The first two siblings (both male) died from respiratory infections at the ages of 7 and 4 months, respectively. Per report of the parents, both of the deceased children had normal birth weights and lengths, and they did not appear dysmorphic. Apart from the index patients (fifth and sixth children), the adult height of all family members was within the normal range for Chilean standards: father, 168 cm; mother, 155 cm; brother, 180 cm; and sister (S1), 157 cm. The siblings are generally healthy. S1 recently developed type 2 diabetes at age 40 but does not have a history of dyslipidemia, thyroid abnormalities, malignancy, or hematological or immunolog-

Table 1. Anthropometric, Clinical, and Biochemical Features of Patients 1 and 2

Parameter	P1	P2	Reference Range
Growth data			
Birth length, cm	45.0 (−2.8 SDS)	46 (−2.3 SDS)	
Birth weight, kg	2.920 (−1.3 SDS)	2.600 (−1.9 SDS)	
Adult height, cm	127.4 (−6.8 SDS)	137.4 (−4.0 SDS)	
Adult arm span, cm	137	145	
Adult weight, kg	33 (−6.9 SDS)	34 (−5.2 SDS)	
Adult BMI, kg/m^2	20.3 (−1.04 SDS)	18.4 (−1.3 SDS)	
Adult head CF, cm	51.3 (−3.3 SDS)	50.5 (−2.9 SDS)	
Clinical signs	Hypergonadotropic hypogonadism T2D, IR, acanthosis Dyslipidemia Clinodactyly Micropenis Bilateral cryptorchidism Cataracts Multinodular goiter	Hypergonadotropic hypogonadism T2D, IR, acanthosis Dyslipidemia Clinodactyly Anemia GIST (jejunum)	
Laboratory data			
Reproductive/pituitary			
LH, mIU/mL	44.6	57	0.6–7.8 (M); 0.5–15.0 (F)
FSH, mIU/mL	62.3	117	0.4–8.7 (M); 0.4–8.6 (F)
T at age 13, ng/dL	10	n.a.	15–500
T at age 18, ng/dL	30	n.a.	265–800
Estradiol, pg/mL	n.a.	13	10–300
IGF-1, ng/mL	195	338	70–454
IGFBP-3, mg/L	3.3	3.8	2.1–4.3
Total T_4, μg/dL	Normal	7.4	4.5–10.9
TSH, μIU/mL	Elevated	3.1	0.4–4.0
Morning cortisol, μg/dL	Normal	12.9	6–23
DHEAS, ng/mL	2392	n.a.	880–3050
Metabolic			
Total cholesterol, mg/dL	168–290	238–309	100–240
LDL, mg/dL	112–189	n.a.	<110
HDL, mg/dL	26–46	47–60	40–59
Triglycerides, mg/dL	172–843	261–579	30–250
HbA1c, %	6.2–12.3	ND	<6.5%
Insulin, fasting, μIU/mL	34	28	8.5–23.0
Insulin, maximum OGTT, μIU/mL	218	180	
Hematological			
WBC, $\times 10^3$/mm^3	6.0	6.4	4.5–11.0
Hemoglobin, g/dL	13	9.7	13–18 (M), 12–17 (F)
Hematocrit, %	37	26–30	43–52 (M), 37–51 (F)
Platelets, $\times 10^3$/mm^3	194	304	140–440
Immunological			
C3	251	249	70–180
C4	34	50	16–45
IgA, mg/dL	176	100	85–385
IgG, mg/dL	681	570	564–1765
IgE, mg/dL	491	50	<87
IgM, mg/dL	73.5	220	45–250
Lymphocyte subpopulations			
WBC, n/mm^3	9.02	n.a.	4.5–11.0
Total lymphocytes, n/mm^3	992 (11%)	n.a.	1442–4239 (16–47%)
CD3– total T cells, n/mm^3	853 (86%)	n.a.	677–2383 (59–83%)
CD4– helper T cells, n/mm^3	367 (37%)	n.a.	424–1509 (31–59%)
CD8– cytotoxic T cells, n/mm^3	466 (47%)	n.a.	169–955 (12–38%)
CD19+ (B cells), n/mm^3	60 (6%)	n.a.	200–400 (11–18%)
CD56+ (NK cells), n/mm^3	50 (5%)	n.a.	200–400 (10–19%)

Abbreviations: CF, circumference; DHEAS, dehydroepiandrosterone sulfate; F, females; HbA1c, hemoglobin A1c; HDL, high-density lipoprotein; IR, insulin resistance; LDL, low-density lipoprotein; M, males; n.a., not available; ND, not determined; T2D, type 2 diabetes; WBC, white blood cells.

ical disease. She has always had regular menses and had three spontaneous pregnancies. Her three children all had normal birth weight and normal childhood growth patterns.

Methods

This study was approved by the Institutional Review Board of the University of Chile. Written informed consent was obtained from the two affected siblings as well as their unaffected sister. Growth charts were generated with GrowthXP software, version 2 (PC PAL).

Genetic analysis

Details of the genetic analysis are provided in the Supplemental Data. For genome-wide single nucleotide polymorphism (SNP) analysis of P1, the Illumina HumanHap300 BeadChip (Illumina, Inc) was used, containing 317 000 TagSNPs, with an average spacing of approximately 9 kb. A total of 750 ng DNA was processed according to the manufacturer's protocol. SNP copy number (log R ratio) and B-allele frequency were assessed using Beadstudio Data Analysis Software version 3.2 (Illumina, Inc). Runs of homozygosity (ROH) scores were calculated using the Copy Number Variation (CNV) partition plug-in (CNV partitioner 1.2.1). The evaluation of CNVs was performed as previously described (14). Candidate gene sequencing was performed using Sanger sequencing for genes involved in the IGF-1 signaling pathway (*IGF1R*, *PIK3R1*, *PIK3R3*, *BMP3*, *PRKG2*) and for the known causes of 3M syndrome (*CUL7*, *OBSL1*, and *CCDC8*). Because *IGF1R* deficiency can also be caused due to a deletion of a large part or the complete coding region, and it is not known what type of mutation to expect in *PIK3R1* and *PIK3R3*, multiplex ligation-dependent probe amplification was performed for these three genes using custom in-house kits to assess for deletions or duplications. Exome sequencing was performed on subjects P1, P2, and S1 at the Cincinnati Children's Hospital Medical Center.

Analysis of XRCC4 cDNA from peripheral blood mononuclear cells (PBMCs) and primary dermal fibroblasts cultures

PBMCs were isolated from blood samples of the unaffected sister (S1) and proband P1. Primary fibroblast cultures of P1, established from a skin biopsy, were maintained as previously described (15). cDNA was amplified and sequenced for XRCC4 as described in the Supplemental Data (reference transcript NM_022406.2).

Microhomology-mediated end-joining (MMEJ) assay

MMEJ assay was employed to evaluate the efficiency of NHEJ using linearized pDVG94 plasmid, as previously described (16). The principle of this assay is to measure the relative efficiency of joining a double-stranded break at a specific location without the loss of a repetitive sequence via the NHEJ pathway vs repair via MMEJ, which results in the loss of one of these repeats. If the repair occurs via MMEJ, a *Bst*XI restriction site is created. *Bst*XI can then be added, and the products can be PCR-amplified and separated by gel electrophoresis. Transfection was carried out using X-tremeGENE HP DNA Transfection Reagent (Roche Diagnostics). Briefly, primary fibroblasts from the proband P1, as well as normal and ligase IV-deficient fibroblasts, were transfected with linearized pDVG94. Extrachromosomal DNA was isolated 48 hours later, and junctions were PCR amplified, followed by restriction enzyme digestion with *Bst*XI. PCR-amplified products were separated by gel electrophoresis and visualized using ethidium bromide.

Results

Genetic analysis

Candidate gene sequencing was performed for a number of genes in the IGF-1 signaling pathway as well as for the known genetic causes of 3M syndrome and produced normal results. These genes were selected since defects in the IGF-1 signaling pathway can lead to microcephalic dwarfism and 3M syndrome causes dwarfism with gonadal failure. A SNP array performed on subject P1 did not reveal any potentially pathogenic CNVs. Homozygosity analysis identified five large ROH located on separate chromosomes, ranging in size from 6.8 to 34 Mb (Supplemental Data). In total, there were 106 Mb of ROH consistent with a coefficient of inbreeding of 1/32 (17), suggesting that the subject's parents were fourth-degree relatives (18).

We next proceeded to perform exome sequencing on subjects P1 and P2 as well as the unaffected sister, S1. Given the SNP array findings, we hypothesized that the causal variant would be a rare variant found in the homozygous state in P1 and P2 and either heterozygous or absent in S1, and that this variant would fall into one of the areas of ROH found in P1. Because the subject's clinical presentation was quite severe, we excluded all variants present in the 1000 Genomes database (www.1000genomes.org) or our internal exome database (~750 individuals) with a minor allele frequency greater than 0.005. There was only a single rare nonsynonymous variant that was homozygous in both P1 and P2 and either heterozygous or absent in S1. As expected, this variant was present in a region of homozygosity found in P1's SNP array. This was a novel variant in exon 3 of *XRCC4*, c.246T>G, which was heterozygous in S1. This variant was confirmed to be homozygous in both P1 and P2 and heterozygous in S1 via Sanger sequencing (Figure 2A). *XRCC4* is an excellent candidate gene because DNA damage repair genes are known to be causal of a number of types of MPD.

cDNA evaluation

The exonic c.246T>G variant is predicted to result in a p.Asp82Glu substitution. Aspartic acid at position 82, however, is not highly evolutionarily conserved, and the p.Asp82Glu missense variant is predicted to be benign by Polyphen2 (http://genetics.bwh.harvard.edu/pph2/) with a score of

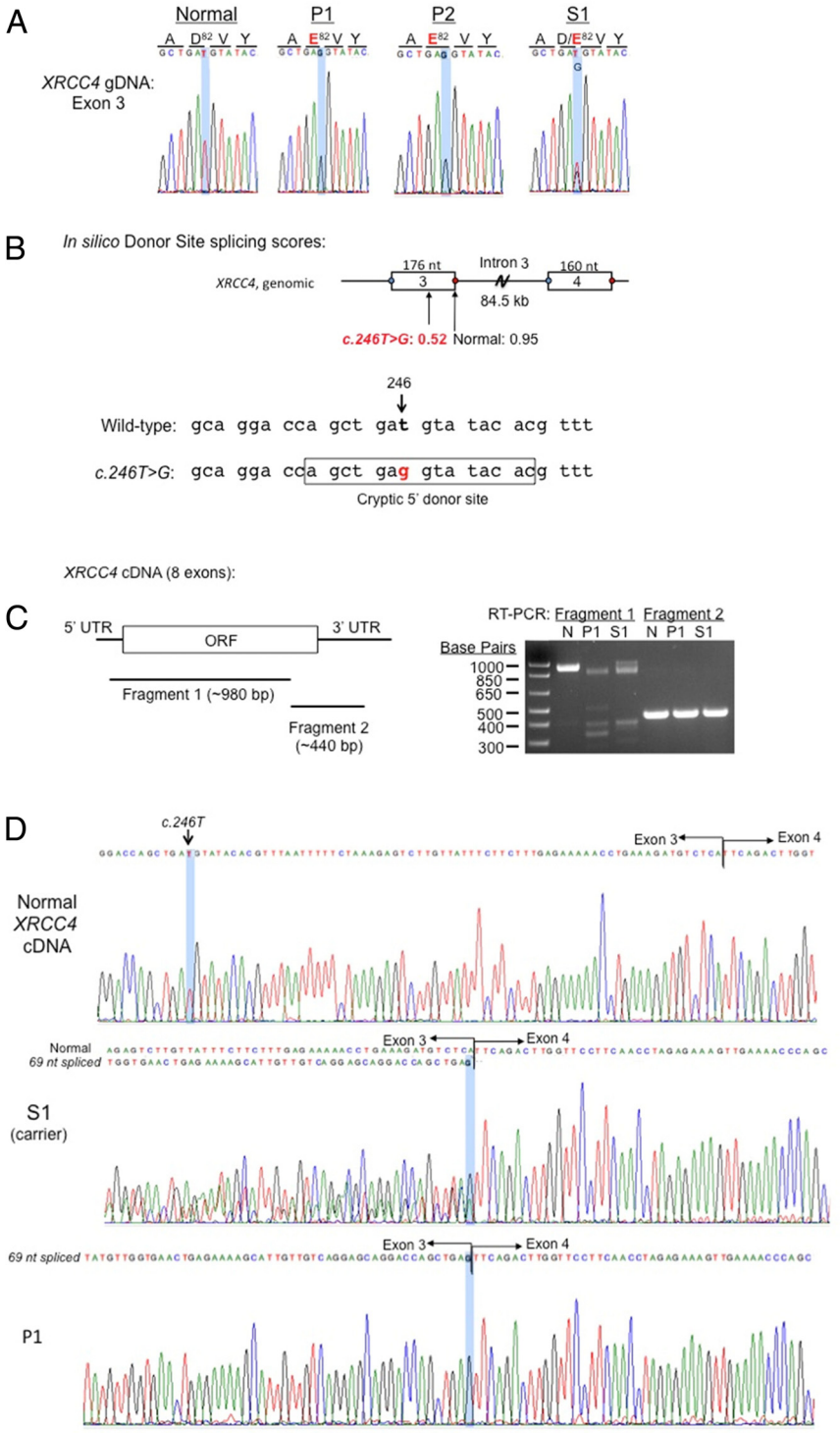

Figure 2. XRCC4 c.246T>G is a splicing mutation. *XRCC4* genomic and cDNA from PBMCs and primary dermal fibroblasts were analyzed. A, Electropherogram confirmed homozygous c.246T>G (highlighted) in P1 and P2 and heterozygosity in carrier S1. Amino acid residues are indicated. B, In silico donor splice site predictions (http://www.fruitfly.org/seq_tools/splice.html). Schematic of exon 3-intron 3-exon 4, donor site score indicated, and sequences corresponding to cryptic 5′ donor site that is generated by C.246T>G, are shown. C, RT-PCR products of XRCC4 cDNA from fresh PBMCs. Coverage of fragments 1 and 2 shown in schematic of XRCC4 cDNA. UTR, untranslated region; ORF, open reading frame that encodes XRCC4 protein; N, normal. D, Sanger sequencing of XRCC4 cDNA. Nucleotide c.246T is highlighted.

0.317 (out of a maximum of 1.0). However, we noted that the T>G transversion could create a new donor splice site with an in silico donor site score of 0.52, which was lower than the in silico donor site score of 0.95 for the normal exon 3 donor splice site (Figure 2B; http://www.fruitfly.org/seq_tools/splice.html). To assess whether the T>G transversion in fact could alter splicing events, we evaluated the *XRCC4* cDNA in PBMC isolated from P1 and S1, compared to normal PBMC. The *XRCC4* cDNA was PCR amplified as two fragments, with fragment 1 encompassing the protein peptide encoded by exons 2–7 (Figure 2C). In normal PBMCs, fragment 1 generated the expected approximately 980-bp PCR product (Figure 2C). P1 PBMC, in contrast, lacked the approximately 980-bp PCR product, with the largest PCR product approximately 900 bp, whereas S1 carried both the approximately 980-bp and approximately 900-bp products (Figure 2C). Fragment 2 from all three PBMC samples was of the same size (~440-bp product) as expected. Sanger sequencing of fragment 1 revealed that P1 carried the homozygous *c.246T>G* variant and deletion of the adjacent 69 base pairs, *c.247_315del*, which corresponded precisely to a splicing event from the novel 5′ donor site (Figure 2D). The aberrant splicing would result in a predicted p.Asp82Glu substitution and an in-frame loss of 23 amino acids (p.Val83_Ser105del). The presence of homozygous *XRCC4* cDNA *c.246T>G* and *c.247_315del* was also observed in primary fibroblasts derived from P1. S1, as expected, was heterozygous for both c.246T>G and *c.247_315del* (Figure 2D).

DNA damage repair functional analysis

We next investigated whether the *XRCC4* mutation conferred a NHEJ defect, employing a MMEJ assay (19) in which linearized pDVG94

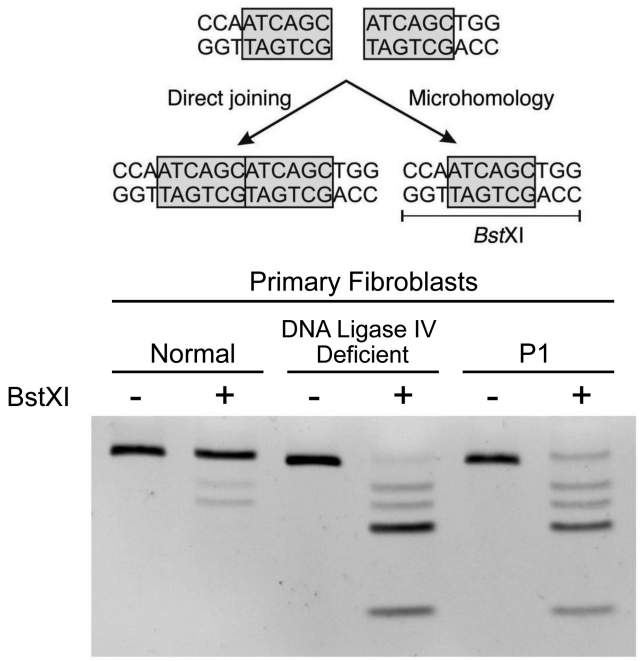

Figure 3. Patient fibroblasts demonstrate a defect in NHEJ. Top, Schematic demonstrating a DSB in the middle of a 6-bp repeat. This can be repaired either via NHEJ (left) or microhomology (right). When repaired via microhomology, a *Bst*XI restriction site is introduced that will result in the generation of multiple shorter DNA bands on the gel. Bottom, MMEJ assay performed in fibroblasts from a normal control, a DNA ligase IV-deficient patient, and proband P1. P1 and the DNA ligase IV-deficient fibroblasts both demonstrate multiple smaller DNA bands after the addition of *Bst*XI, indicating preferential use of the MMEJ pathway for DNA repair.

plasmid DNA was transfected into P1, normal control, and ligase IV-deficient fibroblasts. The 6-bp direct repeat at the junction of the linearized DNA (Figure 3) can be joined either via a functional NHEJ ("direct") pathway or via a microhomology (MMEJ) mechanism, the latter distinguishable by sensitivity to the restriction enzyme *Bst*XI (19). As shown in Figure 3, normal fibroblasts predominantly used the NHEJ pathway (resistant to *Bst*XI digest), whereas the ligase IV-deficient fibroblasts that have severely impaired NHEJ switched almost exclusively to utilizing MMEJ (highly *Bst*XI sensitive). Fibroblasts from P1 show a *Bst*XI digest pattern strikingly similar to that of the ligase IV-deficient fibroblasts, providing functional evidence that the *XRCC4* mutation also severely impaired NHEJ and, therefore, was the most probable cause of the observed phenotype in our patients.

Discussion

In this study we have identified a homozygous single nucleotide variant in the *XRCC4* gene, c.246T>G, as the probable cause of a novel primordial dwarfism syndrome consisting of severe short stature, microcephaly, primary gonadal failure, early-onset metabolic syndrome, and a possible tumor predisposition. We demonstrate that this variant not only resulted in an Asp82Glu exchange but also, importantly, induced a novel, aberrant splicing event that led to the predicted in-frame deletion of 23 amino acids (p.Val83_Ser105del). The biological consequence appears to be a severe impairment in NHEJ-mediated repair of double-stranded DNA breaks (DSBs).

DSBs can be programmed, as for the physiological V(D)J (variable, diverse, joining) recombination process during lymphocyte maturation (20, 21), but more often occur spontaneously or result from exogenous damaging agents such as ionizing radiation or alkylating agents, leading to genomic rearrangements if misrepaired or to cell death when unrepaired (22). Cells use two mechanisms to repair this type of DNA damage: homologous recombination, in which a template of similar DNA sequence is used during the repair; or NHEJ, in which broken DNA ends are directly ligated to each other (21). Efficient NHEJ repair, as might be expected, is a tightly regulated process requiring multiple proteins, including the DNA-dependent protein kinase catalytic subunits, the Ku70/80 heterodimer, Artemis, DNA ligase IV, XRCC4, and NHEJ1 (23). Of these, XRCC4, together with NHEJ1 (alias XLF, XRCC4-like factor) and DNA ligase IV, is involved in the final stages of joining DSBs (20). Based on the three-dimensional crystal structure of known XRCC4-NHEJ1 and XRCC4-DNA ligase IV interactions (24), we hypothesize that loss of the Val83 to Ser105 residues in our mutant XRCC4 specifically disrupted XRCC4-NHEJ1 interactions (XRCC4 contact points include Lys99 and Lys102) and lead to the loss of one of two DNA binding sites formed by the XRCC4-NHEJ1 interactions. This hypothesized loss of function is consistent with the functional studies utilizing primary fibroblasts from P1.

In a murine model, biallelic deficiency in *XRCC4* results in a lethal embryonic phenotype with significant neuronal damage and extensive apoptosis, arrested lymphocyte development, as well as severe growth retardation and reduced fibroblast proliferation rates in vitro (25). Simultaneous knockout of one or both alleles of the *p53* tumor suppressor gene in *XRCC4*-deficient mice rescued the lethal embryonic neuronal phenotype, but these mice do develop pro-B-cell lymphomas at an early postnatal age, and the mice still displayed severe growth retardation, suggesting that XRCC4 deficiency leads to growth failure by a mechanism independent of the neuronal apoptosis (26). Additionally, these mice demonstrate testicular atrophy, thus mimicking the phenotype seen in our patients (27).

To date, there has not been a definitive link between pathogenic *XRCC4* mutations and human disease. How-

ever, in a recent study of genetic causes of primordial dwarfism, Shaheen et al (28) identified a homozygous missense variant in *XRCC4* in a single 4-year-old female with MPD. Functional evidence for the pathogenicity of this missense variant was not provided. This patient exhibited marked short stature (−7.1 SDS) and profound microcephaly. Because the described child is still young, further phenotypic characterization in terms of pubertal growth and development, metabolic abnormalities, and propensity for tumor formation is not known at this time.

Deficiency in a number of the other components of the NHEJ complex including ligase IV, NHEJ1, Artemis, and DNA-dependent protein kinase catalytic subunits has been reported, all leading to a class of disorders entitled radiosensitive, severe combined immunodeficiency (29). Patients with these disorders present with a wide spectrum of immunodeficiency ranging from mild B-cell deficiency with no clinical symptoms to severe neonatal combined immunodeficiency. Many of these patients have short stature and microcephaly as well as a predisposition to lymphoma (29). In a recent paper by Murray et al (30), 11 MPD patients were described with biallelic truncating *LIG4* mutations. This well-phenotyped group of ligase IV-deficiency patients displays a phenotypically diverse spectrum consisting of proportionate intrauterine growth restriction (mean: birth length, −3.8 SDS; birth weight, −3.0 SDS; OFC, −3.6 SDS), severe postnatal growth failure (mean: height, −5.1 SDS; weight, −6.8 SDS), with disproportionate microcephaly (mean: OFC, −10.1 SDS), mild to moderate developmental delay, premature ovarian failure in the peripubertal patients, distinct skin and skeletal abnormalities, as well as facial dysmorphisms (30). Although immunodeficiency was not clinically suspected in 10 of 11 studied patients, most of these patients had hypogammaglobulinemia and decreased B-cell counts, whereas T-cell function appeared to be less affected. In addition to the immunodeficiencies, progressive bone marrow dysfunction was observed in most patients, most notably early-onset thrombocytopenia, but also leukopenia and mild anemia.

In comparison, our two patients with *XRCC4* mutations did not show any signs of clinically significant immune deficiency throughout life. However, upon detailed immunophenotyping, P1 was found to have a number of distinct immunological abnormalities, including mild lymphopenia, an elevated C3 level, and a reduction in B and NK cells. Because NK cells are not part of the adaptive immune system and therefore not directly involved in the process of V(D)J rearrangements, the underlying mechanism is not clear at this time. However, similar NK cell deficiencies have been described in patients with primordial dwarfism due to a mutation in the *MCM4* gene, which is involved in DNA replication and genomic stability (3). Except for a mildly elevated IgE level, P1 had normal Ig levels and normal T-cell subsets. P2 did show a mild, chronic anemia throughout life, which appeared to be due to bone marrow dysfunction after other potential causes such as iron or vitamin deficiencies and hemoglobinopathies had been excluded. Neither of our two patients had documented thrombocytopenia or leukopenia. However, given the wide spectrum of immunodeficiency seen in patients with defects in NHEJ, future immunological studies in patients with *XRCC4* mutations are clearly warranted.

Similar to the two peripubertal ligase IV deficiency patients (30), both of our patients exhibited marked primary gonadal failure (hypergonadotropic hypogonadism) from childhood onward. Both needed complete hormonal replacement therapy for pubertal induction and maintenance of adult secondary sex characteristics. Gonadal failure is seen in other DNA repair syndromes, including the recently described *MCM9* mutation affecting homologous recombination (31). Other well-known primordial dwarfism syndromes are also known to have hypergonadotropic hypogonadism, including the 3M syndrome (32). As stated previously, the murine model of XRCC4-deficient mice also display primary gonadal failure with marked testicular atrophy (27). The above findings clearly indicate the sensitivity of gonadal tissues to the effects of DSBs and the deleterious effects of abnormalities in DNA repair.

A well-known feature of many of the DNA repair syndromes is a marked predisposition for tumor formation, often from an early age onward. Functional defects in NHEJ predispose to genomic rearrangements and chromosomal translocations, which can lead to tumorigenesis (33). P2 developed a rare GIST at the age of 28 years. Because the large majority of GIST tumors (90%) occur in persons over age 40, with a median age of presentation reported between 59 and 63 years, a tumor predisposition phenotype is clearly suggested in her case (34, 35). It has been well described that prior exposure to ionizing radiation in DNA repair syndromes greatly enhances tumor risk and often generates the crucial hit in tumorigenesis. Although P2 had no clear history of ionizing radiation exposure, the significant impairment in DNA damage repair seen in P1's fibroblasts, as well as his family history, strongly suggest that repeated x-ray or computed tomography imaging should be avoided. Most GIST tumors are sensitive to tyrosine kinase inhibitor therapy, but P2 had tumor progression under both imatinib and second-line sunitinib therapy. This may suggest that the tumorigenesis of her GIST could be influenced by the presence of XRCC4 deficiency. Detailed studies of the mutational spectrum in her tumor may provide insights into the lack of treatment response.

The early onset of insulin resistance, type 2 diabetes, and dyslipidemia in both of our patients, in the context of a negative family history, strongly suggests that these metabolic abnormalities are part of the phenotypic spectrum of XRCC4 deficiency. Some of the other dwarfism syndromes, most notably MOPD-2, display a similar clinical picture. Most patients with MOPD-2 develop significant insulin resistance during childhood, leading to acanthosis nigricans and type 2 diabetes mellitus (36). The mechanism behind the marked insulin resistance remains unknown at present. However, in a study by Tavan et al (37), it was shown that mice with a defect in NHEJ and a hypomorphic p53 mutation showed a progressive decrease in pancreatic islet mass independent of apoptosis and innate immunity. The authors concluded that combined DSBs with an absence of p53-dependent apoptosis lead to p53-dependent senescence, diminished β-cell self-replication, depletion of pancreatic islets, and a severe diabetic phenotype. Our patients appear to have insulin resistance as the primary mediator of their diabetes, but it is possible that a similar mechanism is contributing in their cases as well.

Our patients both displayed severe postnatal growth failure, leading to marked short stature of −7 and −4 SDS. There was only minor intrauterine growth restriction, which is different from patients with other underlying causes of primordial dwarfism, including the functionally related ligase IV deficiency. Also, the degree of microcephaly in our patients is less than encountered in the patients with ligase IV deficiency. It is unknown whether this will be a uniform feature of all patients with XRCC4 deficiency or whether our patients have a milder variant.

In conclusion, our study shows that mutations in *XRCC4* add to the wide phenotypic spectrum of DNA repair enzyme syndromes. Although we cannot be certain that this single variant in *XRCC4* accounts for all aspects of our patients' phenotype, it is a clear candidate variant to explain the short stature and gonadal failure and possibly the cancer susceptibility. *XRCC4* mutations may be responsible for a number of patients with unidentified causes of severe short stature and associated primary gonadal failure.

Acknowledgments

We thank Carmen Cao, MD (Hemato-Oncology Service, Clinica las Condes, Santiago, Chile) for assistance with the lymphocyte subpopulation assay.

Address all correspondence and requests for reprints to: Andrew Dauber, Division of Endocrinology, Cincinnati Children's Hospital Medical Center, 3333 Burnet Avenue, MLC 7012, Cincinnati, OH 45229-3039. E-mail: andrew.dauber@cchmc.org.

This work has received funding from the *Eunice Kennedy Shriver* Institute of Child Health and Human Development at the National Institutes of Health (Grants 5K23HD073351, to A.D.; and 1R01HD078592, to V.H.) and the European Community's Seventh Framework Programme (FP7/2007–2013) under Grant Agreement No. HEALTH-F2-2010-259893.

Disclosure Summary: The authors have no conflicts of interest to disclose.

References

1. **Klingseisen A, Jackson AP.** Mechanisms and pathways of growth failure in primordial dwarfism. *Genes Dev*. 2011;25:2011–2024.
2. **Martin CA, Ahmad I, Klingseisen A, et al.** Mutations in PLK4, encoding a master regulator of centriole biogenesis, cause microcephaly, growth failure and retinopathy. *Nat Genet*. 2014;46:1283–1292.
3. **Hughes CR, Guasti L, Meimaridou E, et al.** MCM4 mutation causes adrenal failure, short stature, and natural killer cell deficiency in humans. *J Clin Invest*. 2012;122:814–820.
4. **Bicknell LS, Bongers EM, Leitch A, et al.** Mutations in the pre-replication complex cause Meier-Gorlin syndrome. *Nat Genet*. 2011;43:356–359.
5. **Bicknell LS, Walker S, Klingseisen A, et al.** Mutations in ORC1, encoding the largest subunit of the origin recognition complex, cause microcephalic primordial dwarfism resembling Meier-Gorlin syndrome. *Nat Genet*. 2011;43:350–355.
6. **Kalay E, Yigit G, Aslan Y, et al.** CEP152 is a genome maintenance protein disrupted in Seckel syndrome. *Nat Genet*. 2011;43:23–26.
7. **Gineau L, Cognet C, Kara N, et al.** Partial MCM4 deficiency in patients with growth retardation, adrenal insufficiency, and natural killer cell deficiency. *J Clin Invest*. 2012;122:821–832.
8. **O'Driscoll M, Ruiz-Perez VL, Woods CG, Jeggo PA, Goodship JA.** A splicing mutation affecting expression of ataxia-telangiectasia and Rad3-related protein (ATR) results in Seckel syndrome. *Nat Genet*. 2003;33:497–501.
9. **Ogi T, Walker S, Stiff T, et al.** Identification of the first ATRIP-deficient patient and novel mutations in ATR define a clinical spectrum for ATR-ATRIP Seckel Syndrome. *PLoS Genet*. 2012;8:e1002945.
10. **Qvist P, Huertas P, Jimeno S, et al.** CtIP mutations cause Seckel and Jawad syndromes. *PLoS Genet*. 2011;7:e1002310.
11. **Rauch A, Thiel CT, Schindler D, et al.** Mutations in the pericentrin (PCNT) gene cause primordial dwarfism. *Science*. 2008;319:816–819.
12. **Yan J, Yan F, Li Z, et al.** The 3M complex maintains microtubule and genome integrity. *Mol Cell*. 2014;54:791–804.
13. **Li Z, Pei XH, Yan J, et al.** CUL9 mediates the functions of the 3M complex and ubiquitylates survivin to maintain genome integrity. *Mol Cell*. 2014;54:805–819.
14. **van Duyvenvoorde HA, Lui JC, Kant SG, et al.** Copy number variants in patients with short stature. *Eur J Hum Genet*. 2014;22:602–609.
15. **Fang P, Schwartz ID, Johnson BD, et al.** Familial short stature caused by haploinsufficiency of the insulin-like growth factor I receptor due to nonsense-mediated messenger ribonucleic acid decay. *J Clin Endocrinol Metab*. 2009;94:1740–1747.
16. **Verkaik NS, Esveldt-van Lange RE, van Heemst D, et al.** Different types of V(D)J recombination and end-joining defects in DNA double-strand break repair mutant mammalian cells. *Eur J Immunol*. 2002;32:701–709.
17. **Wierenga KJ, Jiang Z, Yang AC, Mulvihill JJ, Tsinoremas NF.** A clinical evaluation tool for SNP arrays, especially for autosomal

recessive conditions in offspring of consanguineous parents. *Genet Med*. 2013;15:354–360.
18. **Sund KL, Zimmerman SL, Thomas C, et al.** Regions of homozygosity identified by SNP microarray analysis aid in the diagnosis of autosomal recessive disease and incidentally detect parental blood relationships. *Genet Med*. 2013;15:70–78.
19. **van der Burg M, van Veelen LR, Verkaik NS, et al.** A new type of radiosensitive T-B-NK+ severe combined immunodeficiency caused by a LIG4 mutation. *J Clin Invest*. 2006;116:137–145.
20. **Mahaney BL, Hammel M, Meek K, Tainer JA, Lees-Miller SP.** XRCC4 and XLF form long helical protein filaments suitable for DNA end protection and alignment to facilitate DNA double strand break repair. *Biochem Cell Biol*. 2013;91:31–41.
21. **Takata M, Sasaki MS, Sonoda E, et al.** Homologous recombination and non-homologous end-joining pathways of DNA double-strand break repair have overlapping roles in the maintenance of chromosomal integrity in vertebrate cells. *EMBO J*. 1998;17:5497–5508.
22. **Lieber MR.** The mechanism of double-strand DNA break repair by the nonhomologous DNA end-joining pathway. *Annu Rev Biochem*. 2010;79:181–211.
23. **Radhakrishnan SK, Jette N, Lees-Miller SP.** Non-homologous end joining: emerging themes and unanswered questions. *DNA Repair*. 2014;17:2–8.
24. **Hammel M, Rey M, Yu Y, et al.** XRCC4 protein interactions with XRCC4-like factor (XLF) create an extended grooved scaffold for DNA ligation and double strand break repair. *J Biol Chem*. 2011; 286:32638–32650.
25. **Gao Y, Sun Y, Frank KM, et al.** A critical role for DNA end-joining proteins in both lymphogenesis and neurogenesis. *Cell*. 1998;95: 891–902.
26. **Gao Y, Ferguson DO, Xie W, et al.** Interplay of p53 and DNA-repair protein XRCC4 in tumorigenesis, genomic stability and development. *Nature*. 2000;404:897–900.
27. **Chao C, Herr D, Chun J, Xu Y.** Ser18 and 23 phosphorylation is required for p53-dependent apoptosis and tumor suppression. *EMBO J*. 2006;25:2615–2622.
28. **Shaheen R, Faqeih E, Ansari S, et al.** Genomic analysis of primordial dwarfism reveals novel disease genes. *Genome Res*. 2014;24:291–299.
29. **Woodbine L, Gennery AR, Jeggo PA.** The clinical impact of deficiency in DNA non-homologous end-joining. *DNA Repair*. 2014; 16:84–96.
30. **Murray JE, Bicknell LS, Yigit G, et al.** Extreme growth failure is a common presentation of ligase IV deficiency. *Hum Mutat*. 2014; 35:76–85.
31. **Wood-Trageser MA, Gurbuz F, Yatsenko SA, et al.** MCM9 mutations are associated with ovarian failure, short stature, and chromosomal instability. *Am J Hum Genet*. 2014;95:754–762.
32. **Huber C, Munnich A, Cormier-Daire V.** The 3M syndrome. *Best Pract Res Clin Endocrinol Metab*. 2011;25:143–151.
33. **Bunting SF, Nussenzweig A.** End-joining, translocations and cancer. *Nat Rev Cancer*. 2013;13:443–454.
34. **Miettinen M, Makhlouf H, Sobin LH, Lasota J.** Gastrointestinal stromal tumors of the jejunum and ileum: a clinicopathologic, immunohistochemical, and molecular genetic study of 906 cases before imatinib with long-term follow-up. *Am J Surg Pathol*. 2006;30:477–489.
35. **Miettinen M, Sobin LH, Lasota J.** Gastrointestinal stromal tumors of the stomach: a clinicopathologic, immunohistochemical, and molecular genetic study of 1765 cases with long-term follow-up. *Am J Surg Pathol*. 2005;29:52–68.
36. **Huang-Doran I, Bicknell LS, Finucane FM, et al.** Genetic defects in human pericentrin are associated with severe insulin resistance and diabetes. *Diabetes*. 2011;60:925–935.
37. **Tavana O, Puebla-Osorio N, Sang M, Zhu C.** Absence of p53-dependent apoptosis combined with nonhomologous end-joining deficiency leads to a severe diabetic phenotype in mice. *Diabetes*. 2010;59:135–142.